

## Supporting Information

### **Enhanced photoelectric performance of PbS/CdS quantum dots co-sensitized solar cells via hydrogenated TiO<sub>2</sub> nanorod arrays**

Yanli Chen,<sup>a</sup> Qiang Tao,<sup>a</sup> Wuyou Fu,<sup>a</sup> Haibin Yang,<sup>\* a</sup> Xiaoming Zhou,<sup>a</sup> Shi Su,<sup>a</sup>  
Dong Ding,<sup>a</sup> Yannan Mu,<sup>a, b</sup> Xue Li,<sup>a</sup> Minghui Li<sup>a</sup>

<sup>a</sup>State Key Laboratory of Superhard Materials, Jilin University, Changchun 130012, PR China

<sup>b</sup>Department of Physics and Chemistry, Heihe University, Heihe 164300, PR China

Email: yanghb@jlu.edu.cn

## **Experimental section:**

### **Preparation of TiO<sub>2</sub> nanorod arrays photoelectrodes.**

The rutile TiO<sub>2</sub> nanorod arrays film was synthesized by a hydrothermal method, details of the fabrication for TiO<sub>2</sub> nanorod arrays is similar to that described by Liu and Aydil.<sup>1</sup> Typically, 15 ml deionized water was mixed with 15 ml concentrated hydrochloric acid, after it was stirred at ambient conditions for 10 min, 1 ml tetrabutyl titanate was added to the mixture and stirred for another 10 min. The mixture was transferred to a sealed teflon reactor (80 mL volume) after two pieces of cleaned FTO (NSG GROUP, TCO-17, 16Ω/sq, with a thickness of 3.2 mm) substrates were placed within the reactor. The hydrothermal synthesis was conducted at 150 °C in an electric oven for 14 h, then cooled down to room temperature slowly. A white TiO<sub>2</sub> nanorod arrays film was uniformly coated on the FTO glass substrate. The sample was thoroughly washed with DI water and air dried. Finally, the sample was annealed in air at 550 °C for 3 hours to increase the crystallinity of TiO<sub>2</sub> nanorod arrays and improve their contact to the substrate.

### **Hydrogenated treatment.**

TiO<sub>2</sub> nanorod arrays were annealed in hydrogen atmosphere in a range of 250-500 °C, for 30 min. The preparation was performed in a home-built tube furnace filled with ultrahigh purity hydrogen gas (Praxair).

### **Preparation of CdS, PbS co-sensitized TiO<sub>2</sub> nanorod arrays photoelectrodes.**

Successive ionic layer adsorption and reaction (SILAR) was used to prepare CdS and PbS semiconductor sensitizers. In the SILAR process, ethanol and absolute methanol were employed to dissolve Cd(NO<sub>3</sub>)<sub>2</sub> and Pb(NO<sub>3</sub>)<sub>2</sub> as the cation precursor solution. For CdS sensitizer, the TiO<sub>2</sub> photoelectrodes were immersed in a solution containing 0.5 M Cd(NO<sub>3</sub>)<sub>2</sub> in ethanol for 5 min, then sonication-assisted rinsed with ethanol to remove the excess Cd<sup>2+</sup>. The photoelectrodes were dried in a gentle stream of N<sub>2</sub> for 2 min. Subsequently the dried photoelectrodes were dipped into 0.5 M Na<sub>2</sub>S mixed with methanol and deionized water (1:1, v/v) for 5 min. The photoelectrodes were then sonication-assisted rinsed with methanol and dried again with N<sub>2</sub>. All these procedures were considered one SILAR cycle. The incorporated amount of sensitizer

could be increased by repeating the assembly cycle. Preparing PbS sensitizer is similar to CdS, just the concentrations of precursors and the assembly time are minor differences. In preparation of PbS, the photoelectrodes were dipped into the 1 mM  $\text{Pb}(\text{NO}_3)_2$  in absolute methanol for 2 min, and then sonication-assisted rinsed with absolute methanol to remove the excess  $\text{Pb}^{2+}$ . The photoelectrodes were then dried in a gentle stream of  $\text{N}_2$  for 2 min. Subsequently the dried photoelectrodes were dipped into 1 mM  $\text{Na}_2\text{S}$  in absolute methanol for 2 min. The photoelectrodes were then sonication-assisted rinsed with methanol and dried again with  $\text{N}_2$ . For ZnS capping, 0.5 M  $\text{Zn}(\text{CH}_3\text{COO})_2$  in deionized water and 0.5 M  $\text{Na}_2\text{S}$  in deionized water were used for a SILAR process with a dipping time of 10 min each. In this work, all samples prepared were capped with three cycles of ZnS. The resultant products were  $\text{ZnS}/\text{PbS}(x)/\text{CdS}(y)/\text{H-TiO}_2$  ( $\text{TiO}_2$ ), it should be noted that x and y in bracket denote cycles. In addition, ethanol is chosen rather than water here is because ethanol has better wetting and faster evaporation characteristics, which could lead to form better-defined particles through gaps during the  $\text{TiO}_2$  nanorod arrays.<sup>2</sup>

### **Material Characterization**

The morphologies and structure properties of samples were characterized by field-emission scanning electron microscopy (FESEM), high-resolution transmission electron microscopy (HRTEM), X-ray diffraction (XRD), UV-vis diffused reflectance absorption spectra and X-ray Photoelectron Spectroscopy (XPS). FESEM was received on a JEOL JEM-6700F microscope operated at 8 KV. High-resolution transmission electron microscopy (HRTEM) images were obtained on a JEM-2100F microscope with an accelerated voltage of 200 KV. XRD patterns were obtained by conducted on a Rigaku D/max-2500 X-ray diffractometer with  $\text{Cu K}\alpha$  radiation ( $\lambda=1.5418\text{\AA}$ ). UV-vis diffuse reflectance absorption spectra were recorded on a UV-3150 double-beam spectrophotometer. The X-ray Photoelectron Spectroscopy analyses have been performed using a Surface Science Instruments spectrometer (ESCALAB 250) with a focused  $\text{Al K}\alpha$  radiation (1486.6 eV). Electrochemical impedance spectroscopy (EIS) measurements were performed with an CHI650D electrochemical workstation in the frequency of 5 KHz.

### **Photovoltaic characterization**

The photoelectrodes were sealed in sandwich structures with a 25  $\mu\text{m}$  spacer by using Pt catalysts as counter electrode, which were prepared by spreading a drop of 5 mM  $\text{H}_2\text{PtCl}_6$  in 2-propanol on fluorine-doped tin oxide (FTO) glass and heating it to 385  $^\circ\text{C}$  for 15 min in ambient air. The liquid electrolyte composed of 1 M  $\text{Na}_2\text{S}$  and 1 M S solution in Milli-Q ultrapure water was injected between two electrodes. A mask with a window of 0.25  $\text{cm}^2$  was clipped on the  $\text{TiO}_2$  side to define the active area of the cell. Photocurrent–voltage measurement was performed with a Keithley model 2400 Source Meter and a 500W Xe lamp (Spectra Physics) with a monochromator was simulated sunlight. A laser power meter (BG26M92C, Midwest Group) was used to revise the light intensity, as effective as AM 1.5 light at 100  $\text{mW}/\text{cm}^2$ . To eliminate experimental errors, different cells with the same structure were fabricated using the same procedure, and all measurements were carried out five times to confirm the photovoltaic characterization is repeatable in experiments.

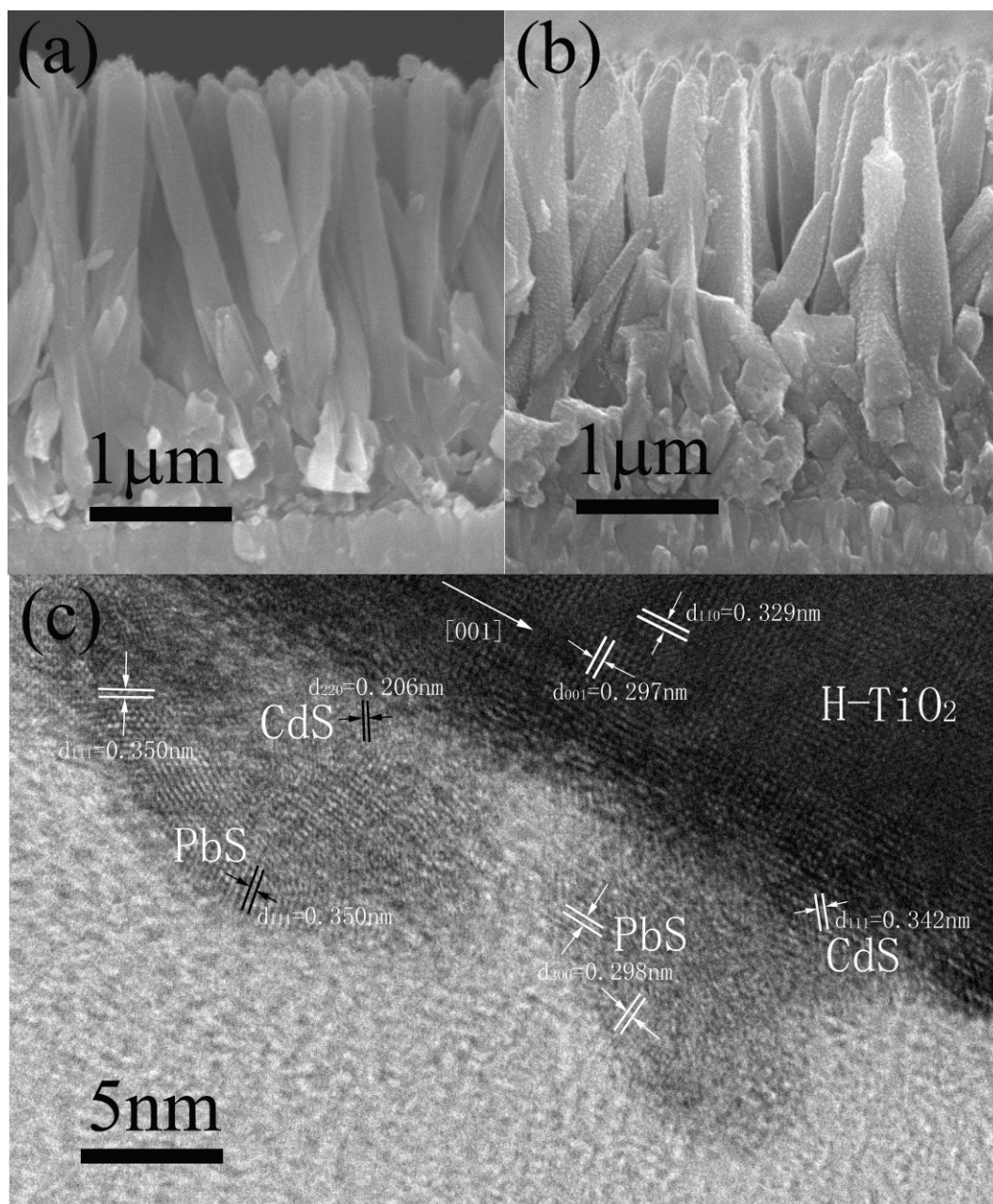


**Fig. S1** Typical SEM and HR-TEM images: (a) the cross-section view of H-TiO<sub>2</sub> nanorod arrays, scale bar is 1 μm; (b) the cross-section view of 6PbS/5CdS/H-TiO<sub>2</sub> nanorod arrays photoelectrodes, scale bar is 1 μm; (c) HR-TEM images of a 6PbS/5CdS/H-TiO<sub>2</sub> nanorod arrays photoelectrodes, scale bar is 5 nm. The samples prepared for FESEM and HRTEM did not cap ZnS for the sake of a better investigation on the growth of CdS and PbS.

The FESEM images of the bare H-TiO<sub>2</sub> nanorod arrays and the 6PbS/5CdS/H-TiO<sub>2</sub> nanorod arrays photoelectrodes are shown in Fig. S1 (a) and (b). Fig. S1 (a) gives the cross-section view of the as-prepared H-TiO<sub>2</sub> nanorod arrays

which obviously shows that the relatively smooth H-TiO<sub>2</sub> nanorod arrays are uniformly formed with rod length of 2.8-3.0 μm and diameter is about 300 nm. Fig. S1 (b) is the H-TiO<sub>2</sub> nanorod arrays after assembled with CdS for 5 cycles and PbS for 6 cycles, the modified H-TiO<sub>2</sub> with rougher surfaces were observed, which reveals that nanocrystals have covered the surfaces of H-TiO<sub>2</sub> nanorod arrays. The detailed microscopic characterization of the 6PbS/5CdS/H-TiO<sub>2</sub> nanostructure was performed by using high-resolution TEM (HR-TEM), which showing that a large amount of CdS and PbS QDs have been deposited on the H-TiO<sub>2</sub> nanorod arrays. From Fig. S1 (c), the heterojunction region indicates the high crystallinity of H-TiO<sub>2</sub>, CdS and PbS. The measured lattice spacings are consistent with the interplanar spacing of H-TiO<sub>2</sub>, CdS and PbS. Lattice fringes with interplanar spacings  $d(110) = 0.329$  nm and  $d(001) = 0.297$  nm are consistent with the rutile phase of TiO<sub>2</sub> [JCPDS no. 21-1276]. While  $d(111) = 0.342$  nm,  $d(220) = 0.206$  nm corresponds to the cubic phase of CdS [JCPDS no. 80-0019],  $d(111) = 0.350$  nm and  $d(200) = 0.298$  nm in accordance with the cubic phase of PbS [JCPDS no. 65-0241].

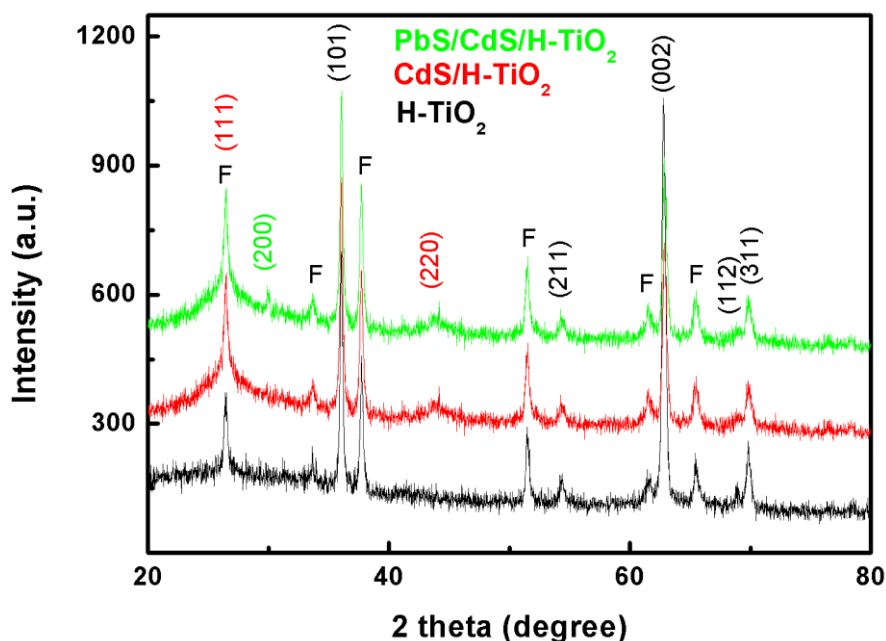


**Fig. S2** XRD patterns of the H-TiO<sub>2</sub>, 5CdS/H-TiO<sub>2</sub> and 6PbS/5CdS/H-TiO<sub>2</sub> photoelectrodes.

Fig. S2 shows the XRD patterns for bare H-TiO<sub>2</sub> nanorod arrays, 5 cycles CdS and 6PbS/5CdS cosensitized H-TiO<sub>2</sub> nanorod arrays. The bare annealed H-TiO<sub>2</sub> nanorod arrays have crystal planes of rutile phases [JCPDS no. 21-1276]. After the sensitization of CdS nanocrystals, new small peaks at  $2\theta$  of  $26.48^\circ$  and  $44.06^\circ$  are exhibited in XRD results. These peaks can be indexed to the (111) and (220) planes of the cubic phase CdS [JCPDS no. 80-0019]. The XRD pattern of 6PbS/5CdS cosensitized H-TiO<sub>2</sub> nanorod arrays exhibit only one small peak at  $30.12^\circ$ , which correspond to the (200) planes of the cubic phase PbS [JCPDS no. 65-0241]. The results are consistent with the HRTEM results above.

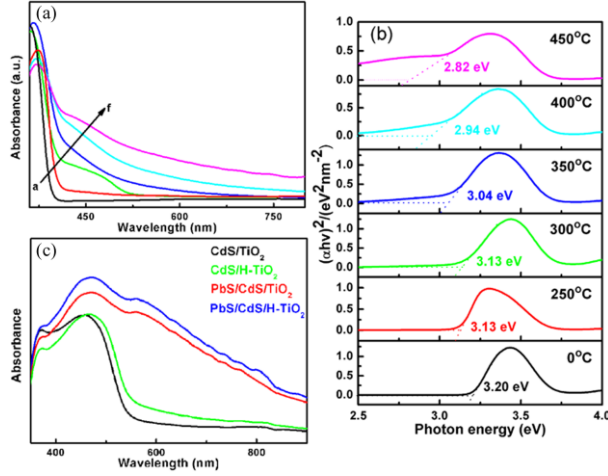


**Fig. S3** Diffuse reflectance absorption spectra (a) the TiO<sub>2</sub> nanorod arrays before and after the H<sub>2</sub> reduction treatment from 250 °C to 450 °C per interval 50 °C (a-f); (b) (αhv)<sup>2</sup>-Photon energy curves for TiO<sub>2</sub> with the H<sub>2</sub> reduction treatment, namely 0, 250, 300, 350, 400 and 450 °C bottom-up, these curves were transformed from the diffuse reflectance absorption spectra, used the form (1) below; (c) TiO<sub>2</sub> and H-TiO<sub>2</sub> nanorod arrays modified with CdS and PbS/CdS QDs.

Fig. S3 (a) shows the UV-vis absorption spectra for the TiO<sub>2</sub> nanorod arrays before and after the H<sub>2</sub> reduction treatment. The pure TiO<sub>2</sub> nanorod arrays can absorb only ultraviolet light with wavelength smaller than 410 nm, because of its large energy gap (~3.2 eV), it can also be confirmed in Fig. S3 (b). However, after the H<sub>2</sub> reduction treatment, the light absorbance extends to visible light region, and the optical absorption in visible region is gradually enhanced with increasing the annealing temperature. The enhanced ability to absorb visible-light of the photoelectrodes makes it be a promising application in photovoltaic devices.

It is well-known that the optical band gap (E<sub>g</sub>) for direct interband transitions and the absorption coefficient (α) near the absorption edge exhibit a relationship of the form<sup>3</sup>

$$(\alpha h\nu)^2 = c(h\nu - E_g) \quad (1)$$

Where c is a constant, ν is the frequency, and h is Planck's constant. The optical band gap can be obtained by extrapolating the linear portion of curves of (αhv)<sup>2</sup>-Photon energy at α=0.

According to the (αhv)<sup>2</sup>-Photon energy curves in Fig. S3 (b), the calculated band

gaps of the H-TiO<sub>2</sub> are narrowed gradually with increase the hydrogenation temperature. So, hydrogenation can narrow the band gap of metal oxide semiconductor.

From Fig. S3 (c), the UV-vis absorption spectra of CdS/TiO<sub>2</sub> and CdS/H-TiO<sub>2</sub> exhibit broad absorption bands from 350 to 570 nm, while in the UV-vis absorption spectra of PbS/CdS/TiO<sub>2</sub> and PbS/CdS/H-TiO<sub>2</sub>, broader absorption bands appear to near-infrared region. In addition, H-TiO<sub>2</sub> samples have slightly wider absorbed region than the samples without hydrogenation. This variation indicates that both QDs and H-TiO<sub>2</sub> can extended the photoresponse into visible light region.

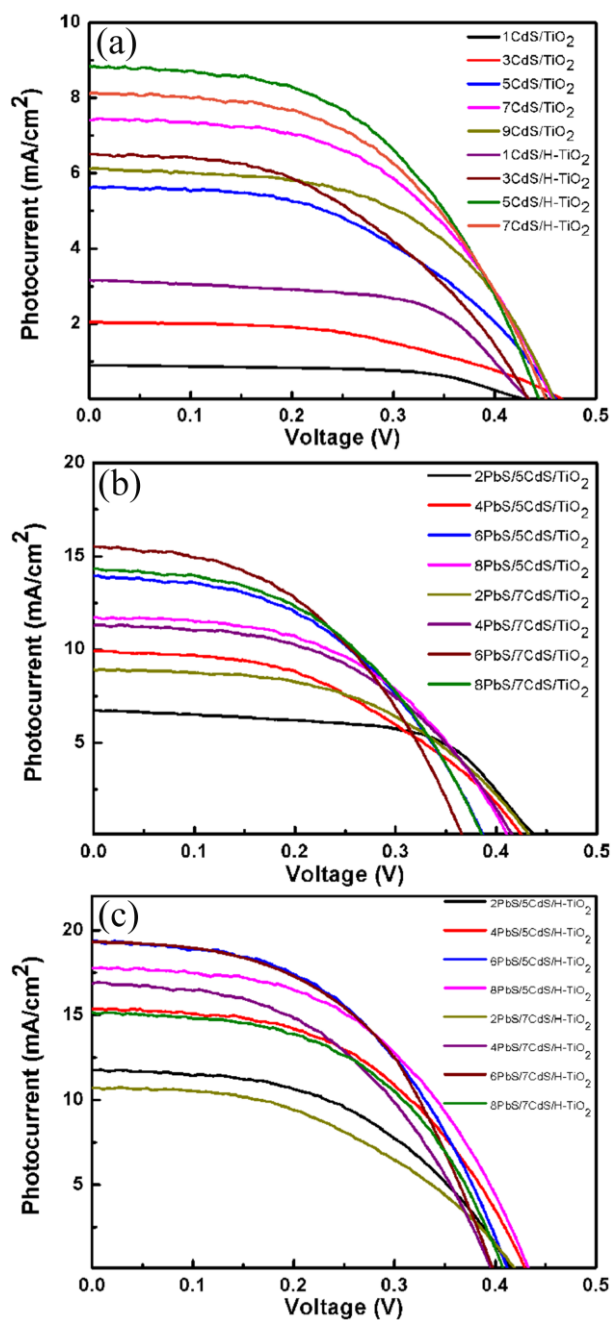


**Fig. S4.** Photocurrent-voltage curves of photoelectrodes with 3 cycles of ZnS as overlayers: (a) TiO<sub>2</sub> and H-TiO<sub>2</sub> photoelectrodes with CdS QDs deposition for different cycles; (b) 5CdS/TiO<sub>2</sub> and 7CdS/TiO<sub>2</sub> photoelectrodes with PbS QDs deposition for different cycles; (c) 5CdS/H-TiO<sub>2</sub> and 7CdS/H-TiO<sub>2</sub> photoelectrodes with PbS QDs deposition for different cycles.

Fig. S4 shows the photocurrent-voltage curves of TiO<sub>2</sub> and H-TiO<sub>2</sub> photoelectrodes with CdS and PbS QDs deposition for different cycles, respectively. The short circuit current density (J<sub>sc</sub>), open circuit potential (V<sub>oc</sub>), fill factor (FF) and

energy conversion efficiency ( $\eta$ ) of all the photoelectrodes are list in Table S1. The bare TiO<sub>2</sub> nanorod arrays photoelectrodes exhibited a stable Jsc of 0.13 mA/cm<sup>2</sup> and Voc of 0.35 V, which resulting in a very low value of energy conversion efficiency (0.01 %). The Jsc was enhanced to 7.41 mA/cm<sup>2</sup> after 7 cycles sensitization with CdS, this Jsc is 57 times more than bare TiO<sub>2</sub> (Table S1). However, it is interesting to note that the Jsc of H-TiO<sub>2</sub> photoelectrodes is 1.48 mA/cm<sup>2</sup>. The results showed that the hydrogen treatment can greatly improve the photoelectric properties of TiO<sub>2</sub>. And the Jsc of CdS/H-TiO<sub>2</sub> nanorod arrays is larger than that of CdS/TiO<sub>2</sub>, which is 8.85 mA/cm<sup>2</sup>. After modified with PbS QDs, the Jsc of TiO<sub>2</sub> and H-TiO<sub>2</sub> are 15.52 mA/cm<sup>2</sup> and 19.34 mA/cm<sup>2</sup>, respectively. The optimum of the conversion efficiency is 3.98 % from 6PbS/5CdS/H-TiO<sub>2</sub>.

**Table S1.** Parameters obtained from the photocurrent-voltage (J-V) curves measurements of multiple semiconductors cosensitized TiO<sub>2</sub> and H-TiO<sub>2</sub> solar cells for different CdS and PbS cycles with 3 cycles of ZnS coating.

Photoelectrodes	Jsc(mA/cm <sup>2</sup> )	Voc(V)	FF(%)	$\eta$ (%)
TiO <sub>2</sub>	0.13	0.35	30.48	0.01
H-TiO <sub>2</sub>	1.48	0.36	30.78	0.16
1CdS/TiO <sub>2</sub>	0.90	0.43	60.08	0.23
3CdS/TiO <sub>2</sub>	2.05	0.47	47.60	0.46
5CdS/TiO <sub>2</sub>	5.60	0.46	47.96	1.24
7CdS/TiO <sub>2</sub>	7.41	0.46	51.95	1.77
9CdS/TiO <sub>2</sub>	6.12	0.46	54.53	1.54
1CdS/H-TiO <sub>2</sub>	3.16	0.43	60.03	0.82
3CdS/H-TiO <sub>2</sub>	6.51	0.43	46.06	1.29
5CdS/H-TiO <sub>2</sub>	8.85	0.44	50.87	1.98
7CdS/H-TiO <sub>2</sub>	8.12	0.45	51.40	1.88
2PbS/5CdS/TiO <sub>2</sub>	6.75	0.44	60.09	1.78
4PbS/5CdS/TiO <sub>2</sub>	9.92	0.43	44.62	1.90
6PbS/5CdS/TiO <sub>2</sub>	13.95	0.39	46.55	2.56
8PbS/5CdS/TiO <sub>2</sub>	11.7	0.41	50.21	2.43

2PbS/7CdS/TiO <sub>2</sub>	8.91	0.43	50.41	1.93
4PbS/7CdS/TiO <sub>2</sub>	11.28	0.42	49.41	2.34
6PbS/7CdS/TiO <sub>2</sub>	15.52	0.37	46.07	2.65
8PbS/7CdS/TiO <sub>2</sub>	14.33	0.39	47.31	2.64
2PbS/5CdS/H-TiO <sub>2</sub>	11.73	0.42	49.41	2.43
4PbS/5CdS/H-TiO <sub>2</sub>	15.35	0.43	50.23	3.32
6PbS/5CdS/H-TiO <sub>2</sub>	19.34	0.42	49.05	3.98
8PbS/5CdS/H-TiO <sub>2</sub>	17.78	0.43	50.41	3.85
2PbS/7CdS/H-TiO <sub>2</sub>	10.72	0.42	45.31	2.04
4PbS/7CdS/H-TiO <sub>2</sub>	16.85	0.39	48.08	3.22
6PbS/7CdS/H-TiO <sub>2</sub>	19.32	0.40	51.28	3.91
8PbS/7CdS/H-TiO <sub>2</sub>	15.16	0.41	52.29	3.24

### References:

- 1 B. Liu, E. S. Aydil, *J. Am. Chem. Soc.*, 2009, **131**, 3985.
- 2 C. H. Chang, Y. L. Lee, *Appl. Phys. Lett.*, 2007, **91**, 053503; H. J. Lee, H. C. Leventis, S. J. Moon, P. Chen, S. Ito, S. A. Haque, T. Torres, F. Nüesch, T. Geiger, S. M. Zakeeruddin, M. Grätzel, M. K. Nazeeruddin, *Adv. Funct. Mater.*, 2009, **19**, 2735.
- 3 R. Gao, L. D. Wang, Y. Geng, B. B. Ma, Y. F. Zhu, H. P. Dong, Y. Qiu, *J. Phys. Chem. C.*, 2011, **115**, 17986; J. J. Tian, R. Gao, Q. F. Zhang, S. G. Zhang, Y. W. Li, J. Lan, X. H. Qu, G. Z. Cao, *J. Phys. Chem. C.*, 2012, **116**, 18655; R. Zhou, Q. F. Zhang, J. J. Tian, D. Myers, M. Yin, G. Z. Cao, *J. Phys. Chem. C.*, 2013, **117**, 26948.